Supporting Information

Electrocatalytic water oxidation by a water-soluble copper complex with a pentadentate amine-pyridine ligand

Ziyi Xu,[‡a] Zilin Zheng,[‡a] Qi Chen,[a] Jiayi Wang,[a] Kaishan Yu,[a] Xin Xia,[a] Junyu Shen[*a,b] and Qijian Zhang[*a]

[a] *Jiangsu Laboratory of Advanced Functional Materials, School of Materials Engineering, Changshu Institute of Technology, Changshu 215500, P. R. China.*

[b] *Changshu Research Institute, Dalian University of Technology, Changshu 215500, P. R. China.*

‡ *These authors contributed equally to this work.*

* *Corresponding author, E-mail: shenjunyu2014@126.com (Junyu Shen)*

Materials: Commercially available chemicals, $Cu(BF_4)_2 \cdot 6H_2O$, $Zn(BF_4)_2$, dichloromethane, magnesium sulfate, sodium hydrogen carbonate, sodium triacetoxyborohydride, sodium phosphate tribasic, sodium phosphate dibasic dodecahydrate, sodium acetate, boracic acid, sodium hydroxide, 2,6-pyridinedicarboxaldehyde and methyl(2-pyridylmethyl)amine were purchased from Adamas Reagent and used as received. Glassy carbon electrode, fluorine-doped tin oxide (FTO) glass plate, and platinum wire were purchased from Tianjin Gaoss Union for the electrochemical studies. All buffers were prepared with deionized water (18 MΩ-cm resistivity).

Instruments: NMR Spectra were collected with a Varian INOVA 500 NMR

spectrometer. Mass spectra were recorded with HP 1100 HPL/ESI-DAD-MS and Waters/Micromass LC/Q-TOF-MS instruments. Elemental analyses were performed with a Thermoquest-Flash EA 1112 elemental analyzer. UV-Vis absorption measurements were carried out on an Agilent 8453 spectrophotometer. SEM images and EDX spectra were obtained with a HITACHI UHR FE-SEM SU8220 instrument equipped with an EDX detector. XPS surveys were acquired with a Thermo Fisher ESCALAB 250Xi surface analysis system. The measurements of dynamic light scattering (DLS) spectra were measured with a Zetasizer Nano ZS90 instrument.

Crystallographic structure determinations. The single-crystal X-ray diffraction data were collected on a Bruker Smart Apex II CCD diffractometer with a graphite-monochromated Mo-K_α radiation (λ = 0.071073 Å) at 296 K using the ω-2θ scan mode. Data processing was accomplished with the SAINT processing program.[S1] Intensity data were corrected for absorption by the SADABS program.[S2] All structures were solved by direct methods and refined on F^2 against full-matrix least-squares methods by using the SHELXTL 97 program package.[S3] Non-hydrogen atoms were refined anisotropically. Hydrogen atoms were located by geometrical calculation. Crystallographic data and selected bond lengths and angles for **1** are given in Tables S1 and S2 (CCDC- 2020089 for **1**).

CV experiments. Cyclic voltammetry experiments were carried out in a three-electrode cell under argon. The working electrode was a glassy carbon electrode

disc (0.071 cm^2), the reference electrode was an aqueous Ag/AgCl electrode, and the counter electrode was a platinum wire. The solution of 0.1 M phosphate buffer at pH 11.0 was used as supporting electrolyte, which was degassed by bubbling with argon for 15 min before measurement. All potentials are reported versus the normal hydrogen electrode (NHE) by addition of 0.197 V to the experimentally measured values.

CPE experiments. The controlled potential electrolysis (CPE) experiment was carried out in a home-made H-type electrochemical cell with an FTO (1.0 cm^2) glass slide as working electrode. The auxiliary electrode was a platinum wire which was protected by a casing pipe and the reference electrode was a commercially available aqueous Ag/AgCl electrode. The sample was bubbled with argon for 20 min before measurement with constantly stirring.

The determination of FE. The Faradaic efficiency (FE) was determined from CPE experiment of the solutions of **1** in 0.1 M phosphate buffer at pH 11.0 in a custom-built gas-tight electrochemical cell at an applied potential of 1.6 V vs NHE for 3 h. The gas in the headspace of the cell was analyzed by CEAULIGHT GC-7920 gas chromatograph equipped with a 5 Å molecular sieve column (2 mm $\times$ 2 m) during the electrolysis and the oxygen dissolved in the solution was neglected. Faradaic efficiencies of electrochemical O$_2$ evolution were determined according to the amount of O$_2$ evolved and the amount of O$_2$ calculated from the total consumed charge during

the CPE experiment by assuming a 4e⁻ catalytic process (eq. 1).

$$FE = \frac{\text{Produced O}_2 \text{ (n}_{\text{measured}})}{\text{Calculated O}_2 \text{ (n}_{\text{caculated}})} \times 100\%$$

(eq.1)

Produced oxygen was obtained from peak area of gas chromatograph and standard curve of O_2. Calculated oxygen can be got through the eq. 2:

$$n_{\text{caculated}} = \frac{Q}{n \times e \times NA}$$

(eq.2)

Where Q is the total amount of charge consumed during electrolysis, n is number of electron transferred for water oxidation ($n = 4$), e is the elementary charge ($e = 1.6 \times 10^{-19}$ C), NA is Avogadro constant ($NA = 6.02 \times 10^{23}$).

Kinetic equations.

$$i_d = 0.4463 n_d FA[\text{Cu}](n_d FvD_{\text{Cu}}/RT)^{1/2} \qquad \text{(eq. 3)}$$

$$i_c = n_c FA[\text{Cu}](k_{\text{cat}} D_{\text{Cu}})^{1/2} \qquad \text{(eq. 4)}$$

$$i_c/i_d = 2.24 n_c n_d^{3/2} (k_{\text{cat}} RT)^{1/2} (Fv)^{-1/2} \qquad \text{(eq. 5)}$$

where i_d is the plateau current density of noncatalytic wave (here taken from the peak current of Cu^I to Cu^{II}), n_d is the number of electron transferred for the Cu^I/Cu^{II} couple ($n_d = 1$), v is the scan rate, R is the universal gas constant, and T is the temperature in Kelvin ($T = 298.15$ K), i_c is the limiting catalytic peak current, n_c is the number of electrons transferred for producing a molecule of O_2 in water oxidation ($n_c = 4$), F is Faraday constant, A is the surface area of the electrode (in cm²), [Cu] is the initial concentration of catalyst (in mol L⁻¹), k_{cat} is the apparent first-order rate constant, and D_{Cu} is the diffusion coefficient of the copper catalyst in 0.1 M phosphate
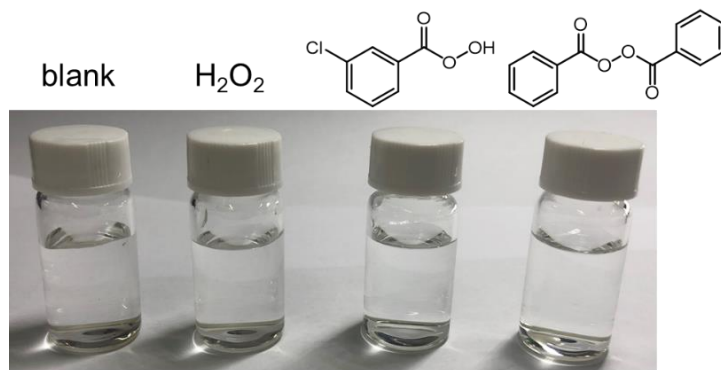
buffer solution at pH 11.0.

Substituting data into eq. 5, it could be simplified to eq. 6.

$$i_c/i_d = 1.436(k_{cat}/v)^{1/2} \qquad \text{(eq. 6)}$$

Testing peroxide intermediates formed during CPE experiments in electrolytes.

Ampliflu red (AR) was dissolved in DMSO and horseradish peroxidase (HRP) in 0.5 M PBS, both in a concentration of 0.4 mg mL^{-1}. The controlled potential electrolysis (CPE) experiment of **1** (1 mM) in 0.1 M PBS at pH 11 was carried out at 1.6 V vs. NHE in an electrochemical cell with cathode and anode isolated by a porous ceramic frit. A fluorine-doped tin oxide (FTO) with a surface area of 1.5 cm^2 was used as working electrode. After 3 h of electrolysis, the HRP solution (1.0 mL) and AR solution (1.0 mL) were successively added into the resulting electrolyte (0.3 mL). The blue color of the solution turned pink after the sample was shaken for about 1 minute (Figure S18).

This chromogenic reaction is always applied in the detection of hydrogen peroxide, so we do some experiments to confirm whether this method is applicable to other peroxide. The hydrogen peroxide, 3-chloroperoxybenzoic acid and benzoyl peroxide are chosen as substrates, the test results are shown in the following picture. The solution of compound containing perhydroxyl (-OOH) turns pink after the addition of HRP and AR (The substrates were dissolved in acetonitrile). This experimental phenomenon means that this chromogenic reaction is suitable for the detection of -OOH probably.

blank   H₂O₂

+HRP, +Ar

R-OOH $\xrightarrow{\text{HRP}}$ HO •
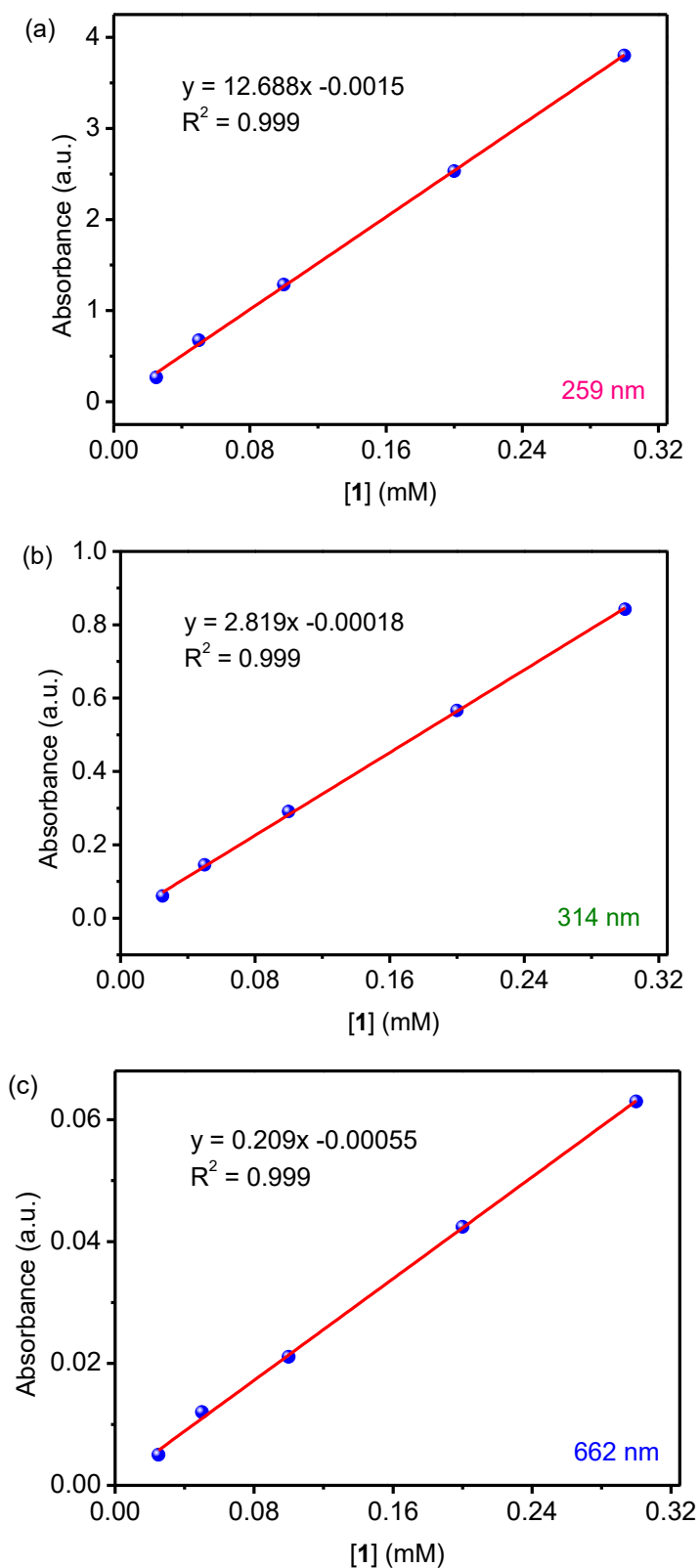
Ampliflu red (colorless)   Resorufin (red)
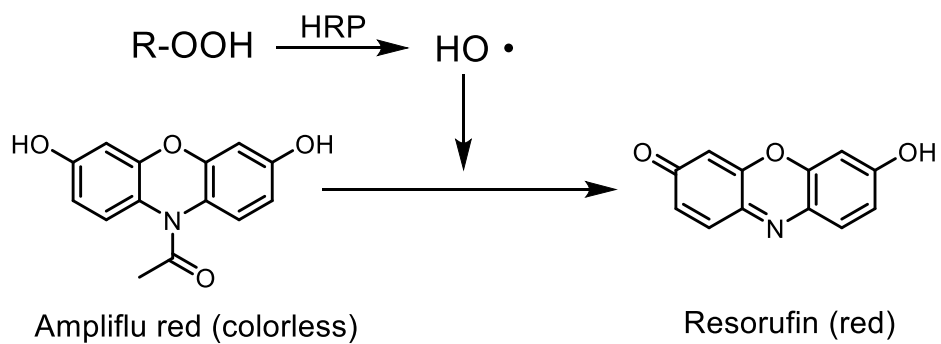
Figure S1. Plots of the absorbance intensity at 259 nm (a), 314 nm (b) and 662 nm (c) versus the concentration of **1** (from 0.025 to 0.300 mM).
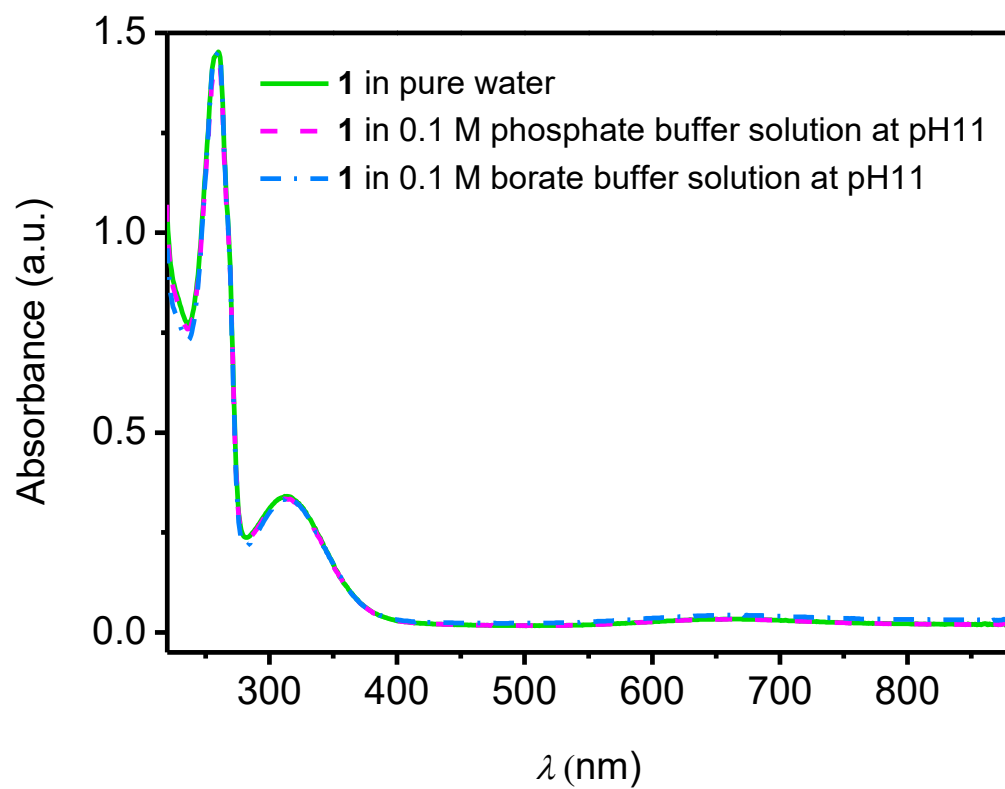
Figure S2. UV-vis spectra of **1** (0.1 mM) in pure water, 0.1 M phosphate buffer and borate buffer solutions at pH 11 (optical length: 10 mm).
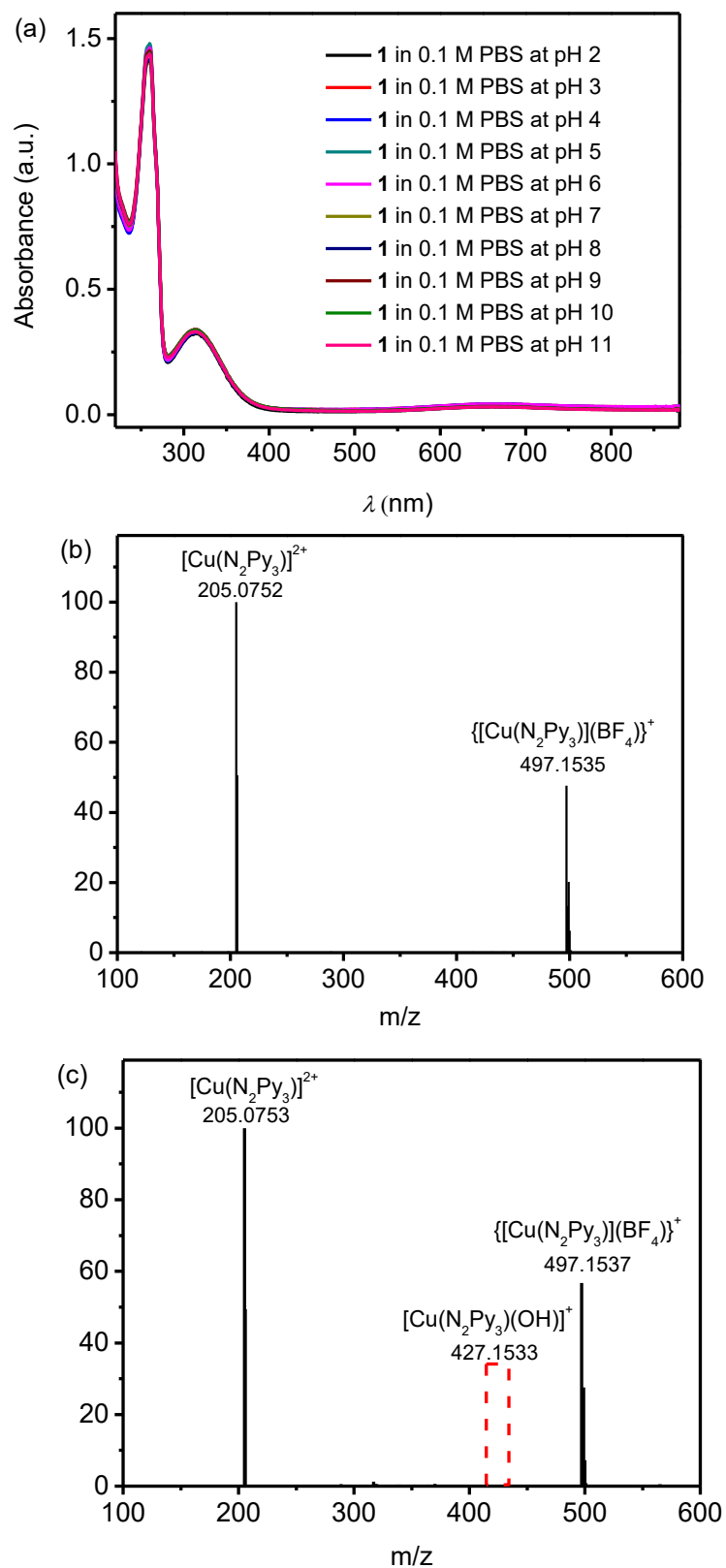
Figure S3. (a) UV-vis spectra of **1** (0.1 mM) in 0.1 M PBS at different pH (optical length: 10 mm). HRMS of **1** in pure water (b) and NaOH solution at pH 11 (c).
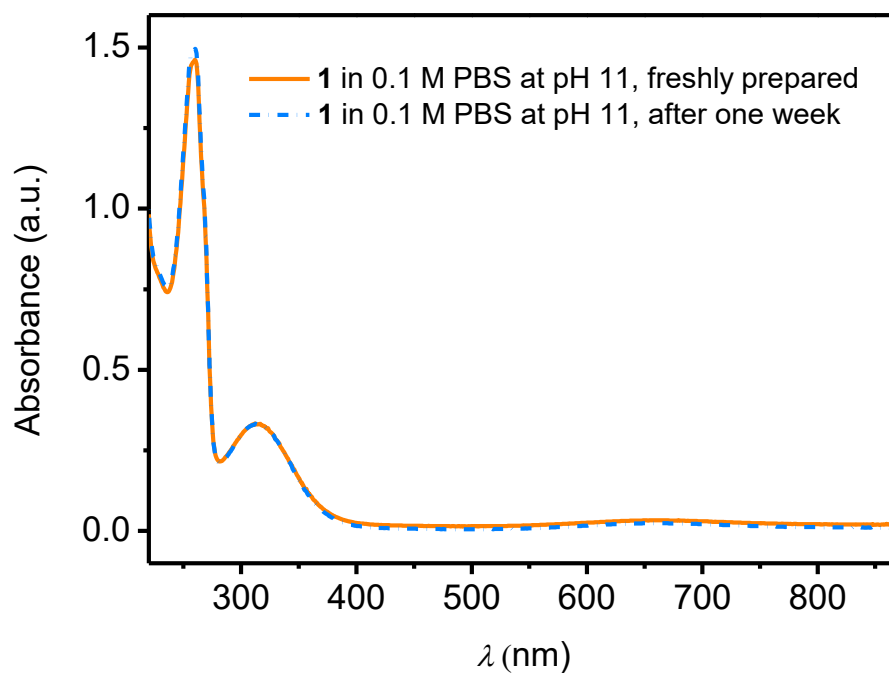
Figure S4. Comparison of UV-vis spectra of **1** (0.1 mM) in 0.1 M PBSs measured when freshly prepared and after stood for a week under air (optical length: 10 mm).
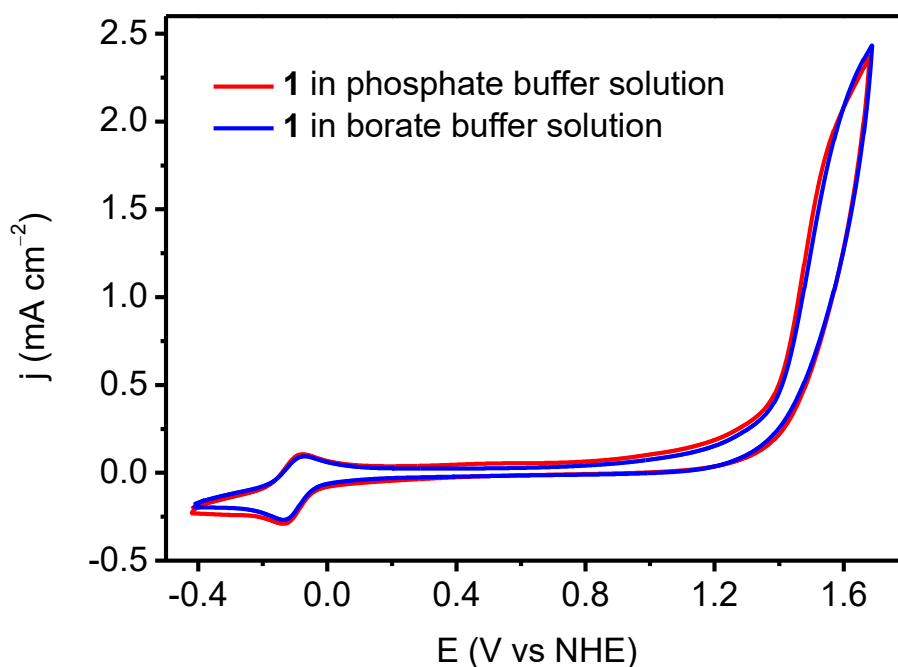
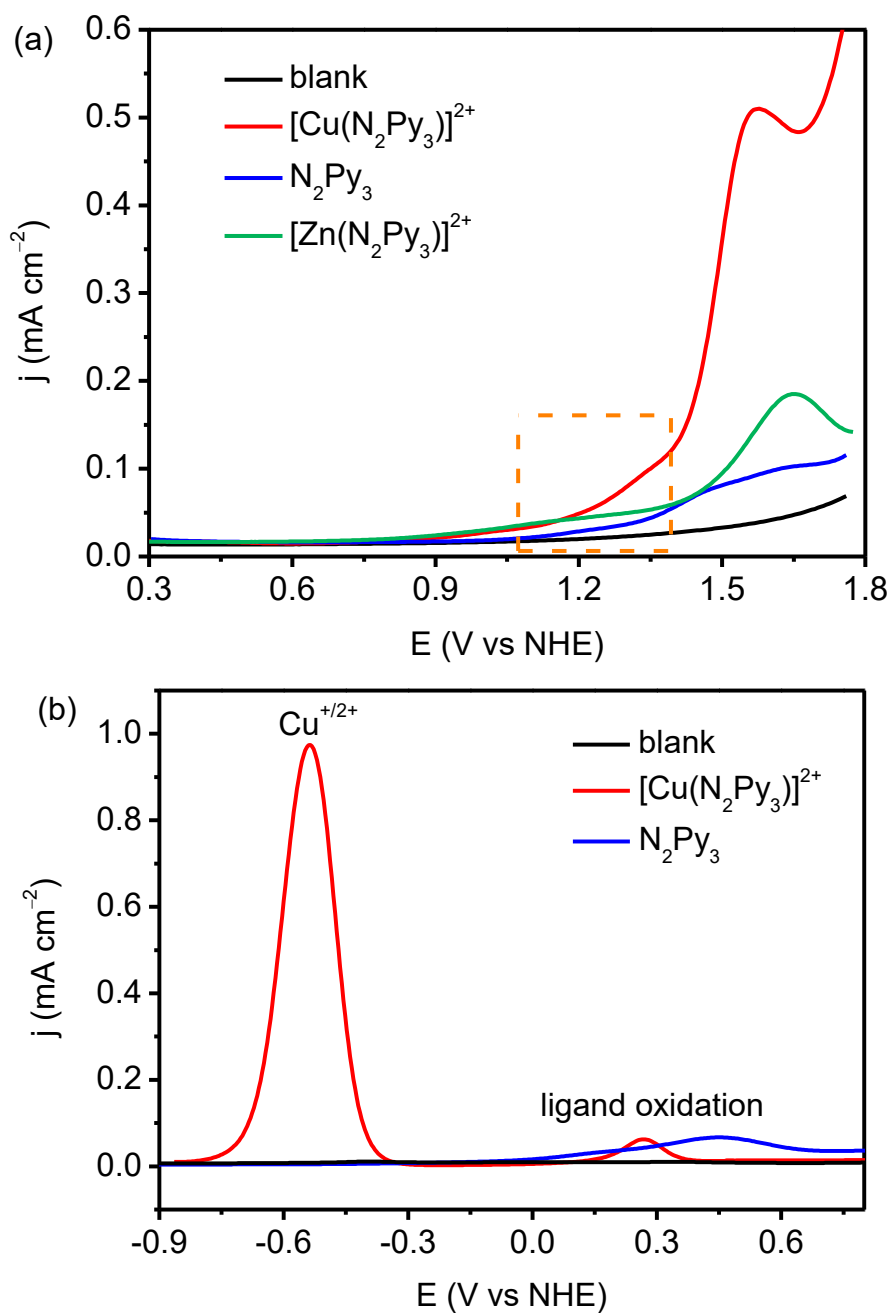**Figure S5.** CV curves of **1** (1.0 mM) in 0.1 M phosphate buffer and borate buffer solutions at pH 11 at a scan rate of 100 mV s^{-1}.

Figure S6. (a) DPV curves of blank, **1**, N_2Py_3 and $[Zn(N_2Py_3)]^{2+}$ (all in 1.0 mM) in

0.1 M PBSs at pH 11 at a scan rate of 8 mV s^{-1}. (b) SWV curves of blank, **1** and

N_2Py_3 (both in 1.0 mM) in CH$_3$CN at a scan rate of 4 mV s^{-1} under nitrogen.
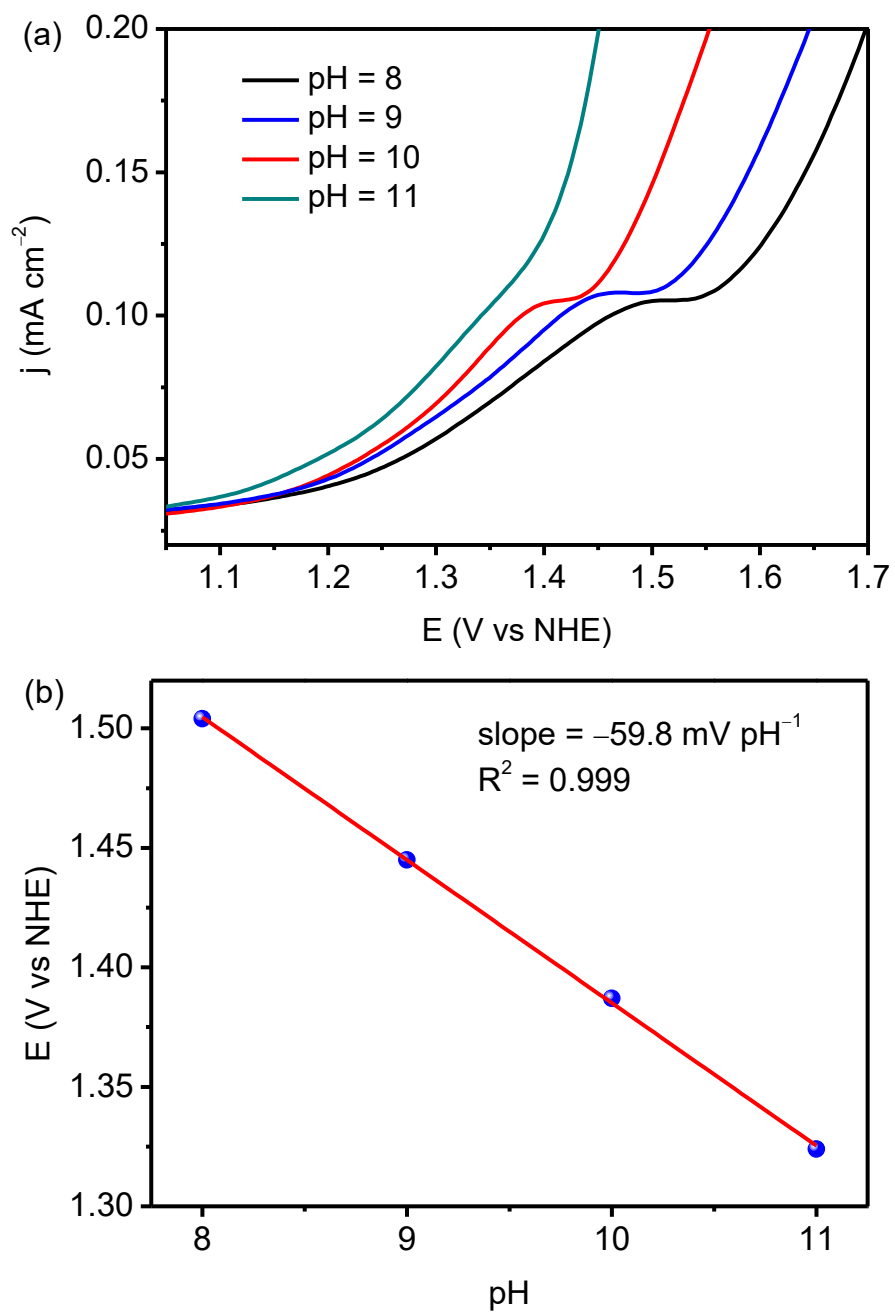
Figure S7. (a) DPV of **1** (1.0 mM) in 0.1 M PBSs with pH varied from 8 to 11. (b) Pourbaix plots for **1**.
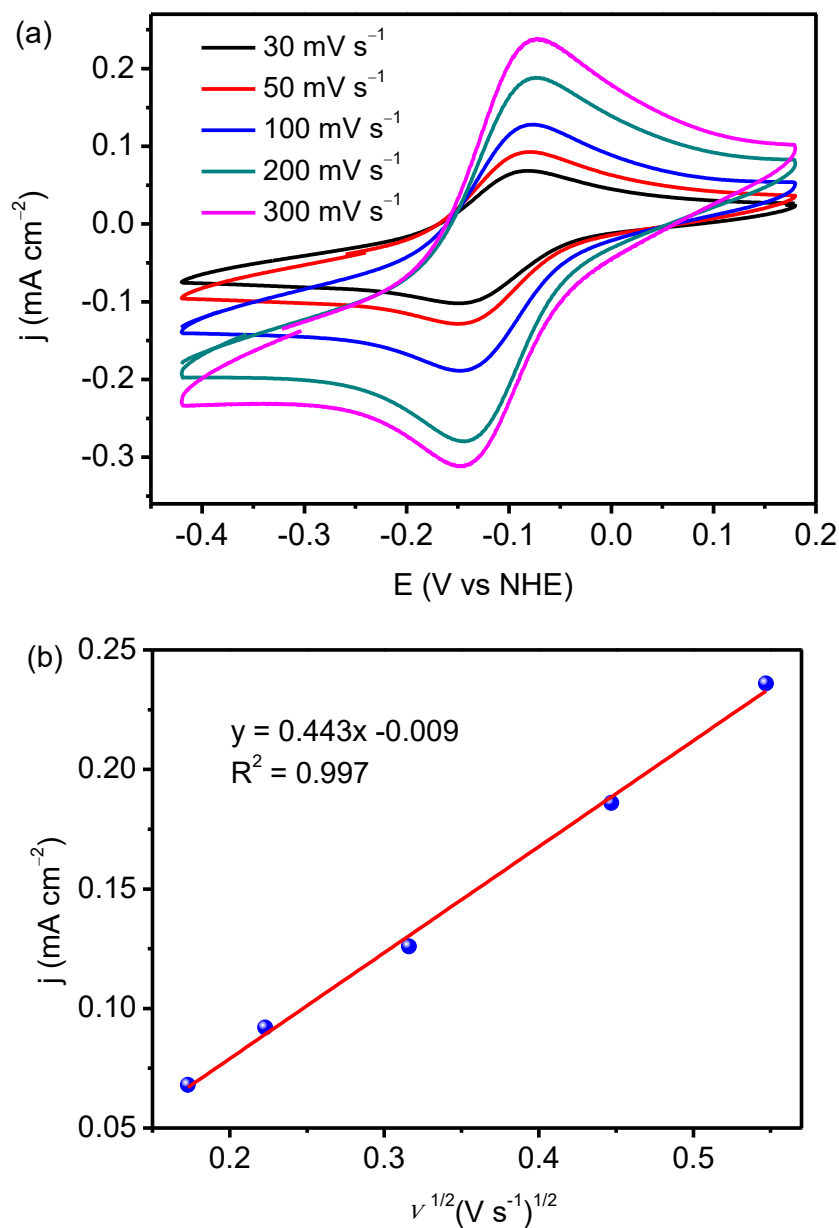
Figure S8. (a) Cyclic voltammograms of **1** (1.0 mM) in 0.1 M PBSs at pH 11 with scan rate varying from 30 to 300 mV s^{-1}. (b) Plot of the anodic current density maximum of the Cu^{I}/Cu^{II} couple as a function of the square root of scan rate.
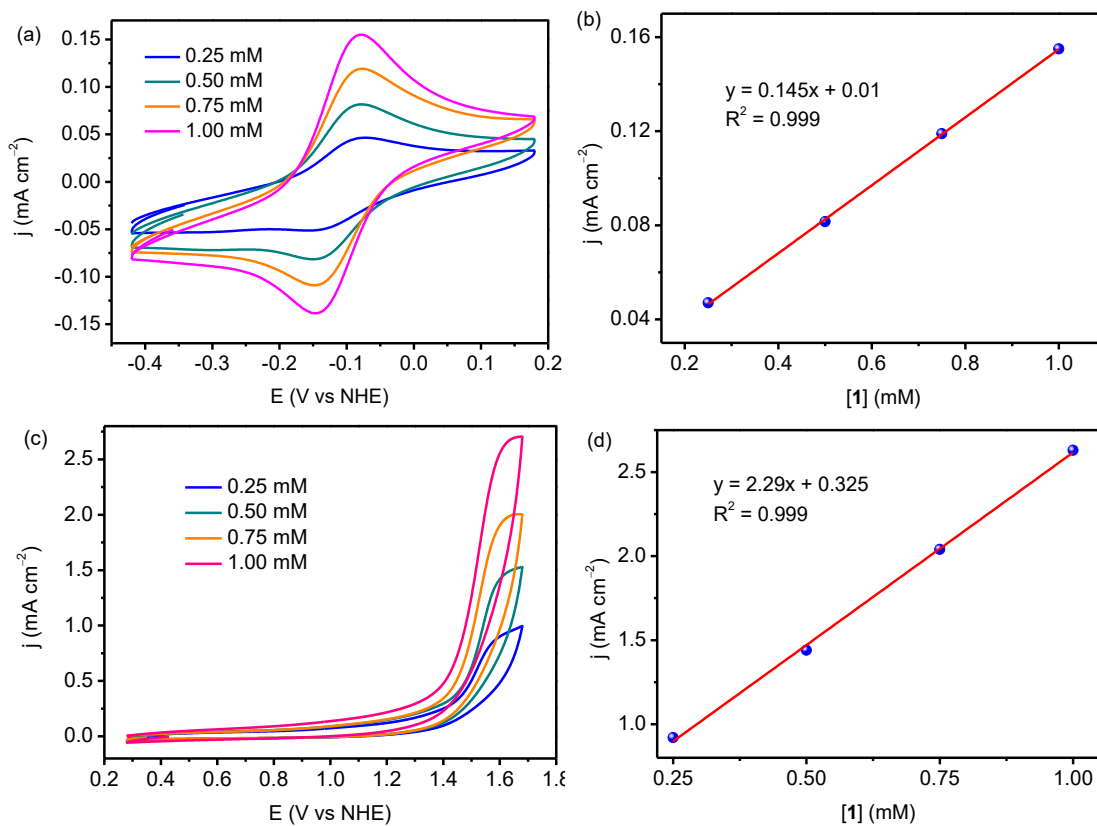
Figure S9. (a) Cyclic voltammograms of **1** in 0.1 M PBSs at pH 11 at a scan rate of 100 mV s^{-1} with the concentration of **1** varying from 0.25 to 1.00 mM (scan range from −0.42 to 0.18 V). (b) Plots of the current density maxima (j_d), as a function of catalyst concentration. (c) Cyclic voltammograms of **1** in 0.1 M PBSs at pH 11 at a scan rate of 100 mV s^{-1} with the concentration of **1** varying from 0.25 to 1.00 mM (scan range from 0.28 to 1.68 V). (d) Plots of the current density maxima (j_c), as a function of catalyst concentration.
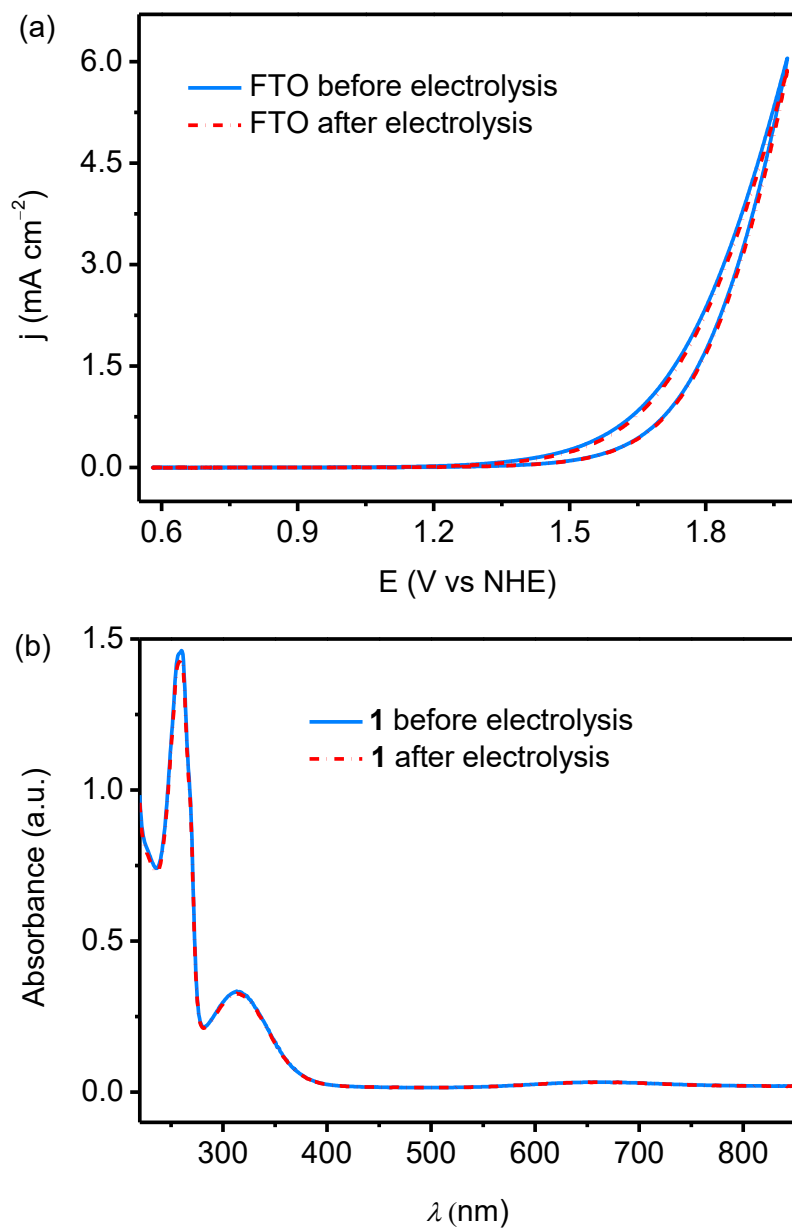
Figure S10. (a) CVs of **1** (1.0 mM) in 0.1 M PBSs at pH 11 at a scan rate of 100 mV s^{-1} with an FTO electrode (1 cm^2) before and after electrolysis. (b) UV-vis spectra of **1** (both in 0.1 mM) in 0.1 M PBSs at pH 11 before and after electrolysis (optical length: 10 mm).
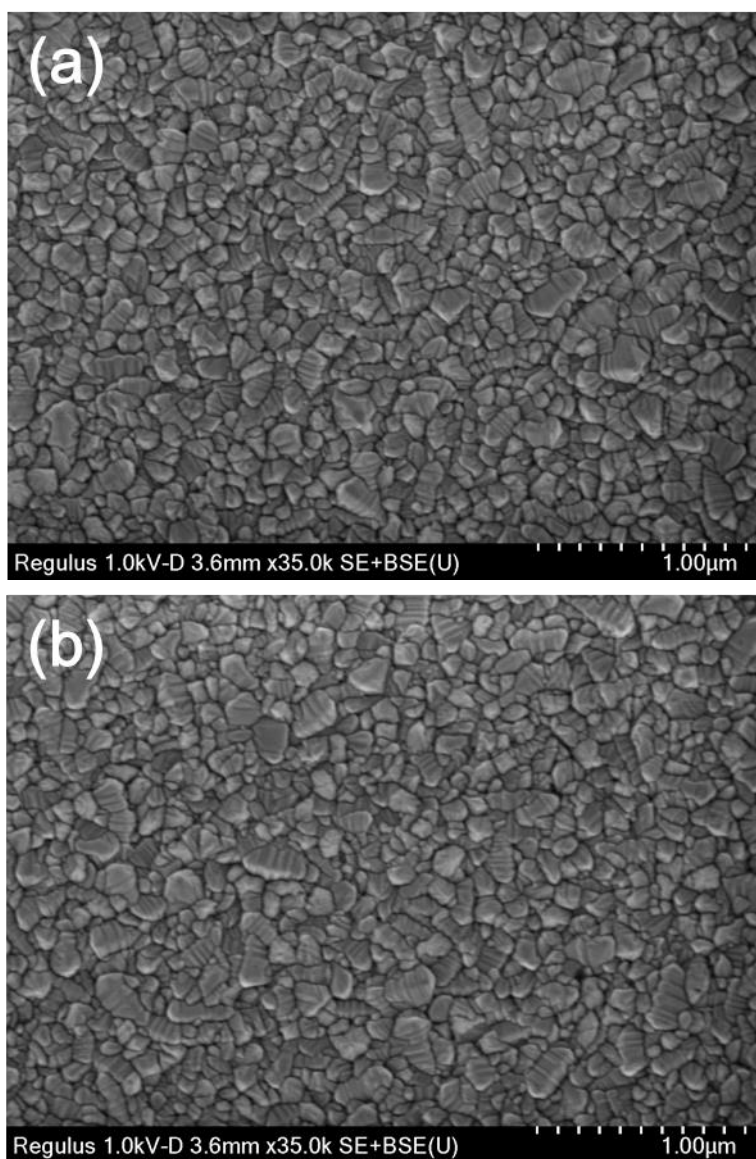
Figure S11. SEM images of FTO before (a) and after 3 h of CPE experiment (b) with **1** as catalyst.
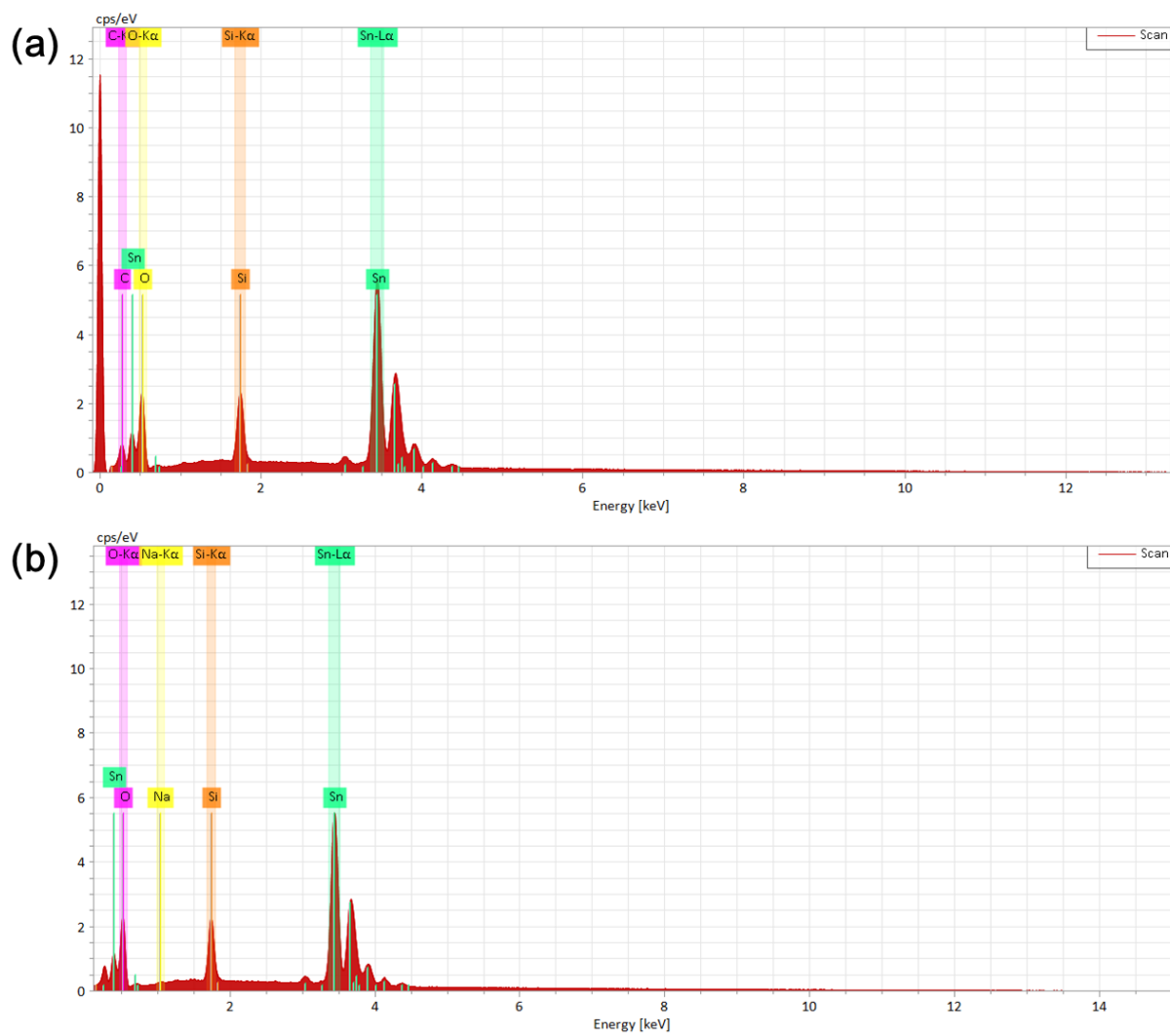
Figure S12. EDX spectra of FTO before (a) and after 3 h of CPE experiment (b) with **1** as catalyst.
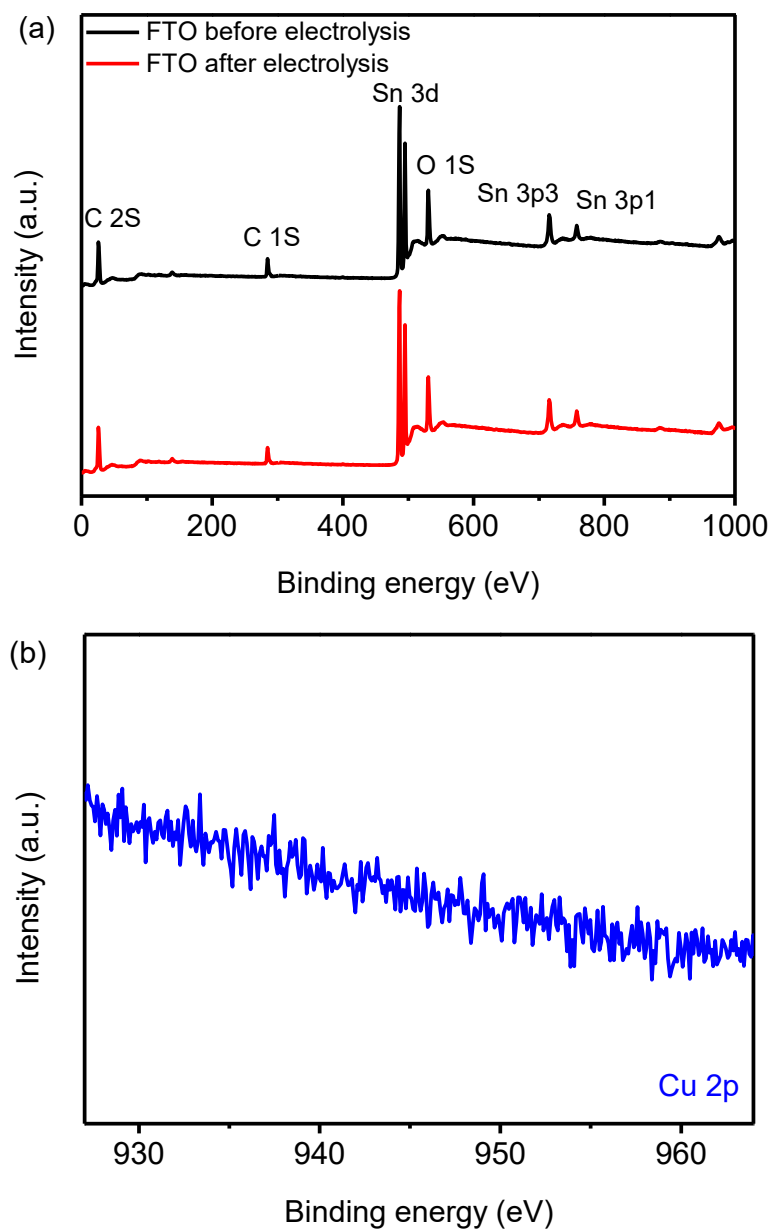
Figure S13. (a) XPS surveys of FTO before and after 3 h of CPE experiment with **1** as catalyst. (b) XPS spectra of Cu 2p for FTO after 3 h electrolysis with **1** as catalyst.

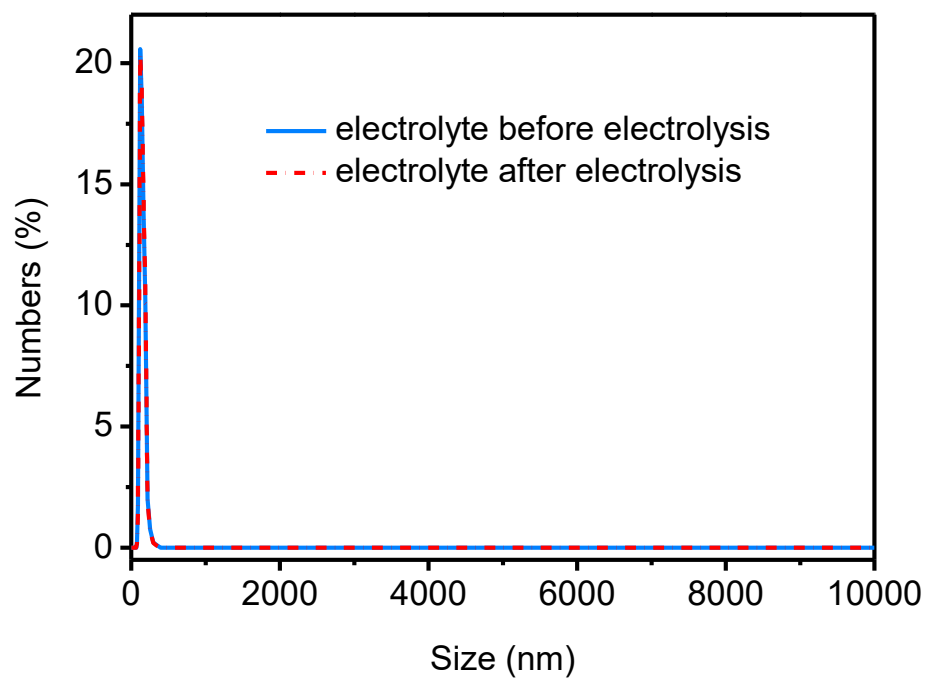**Figure S14.** DLS spectra of electrolytes before and after 3 h of electrolysis with **1** as catalyst.
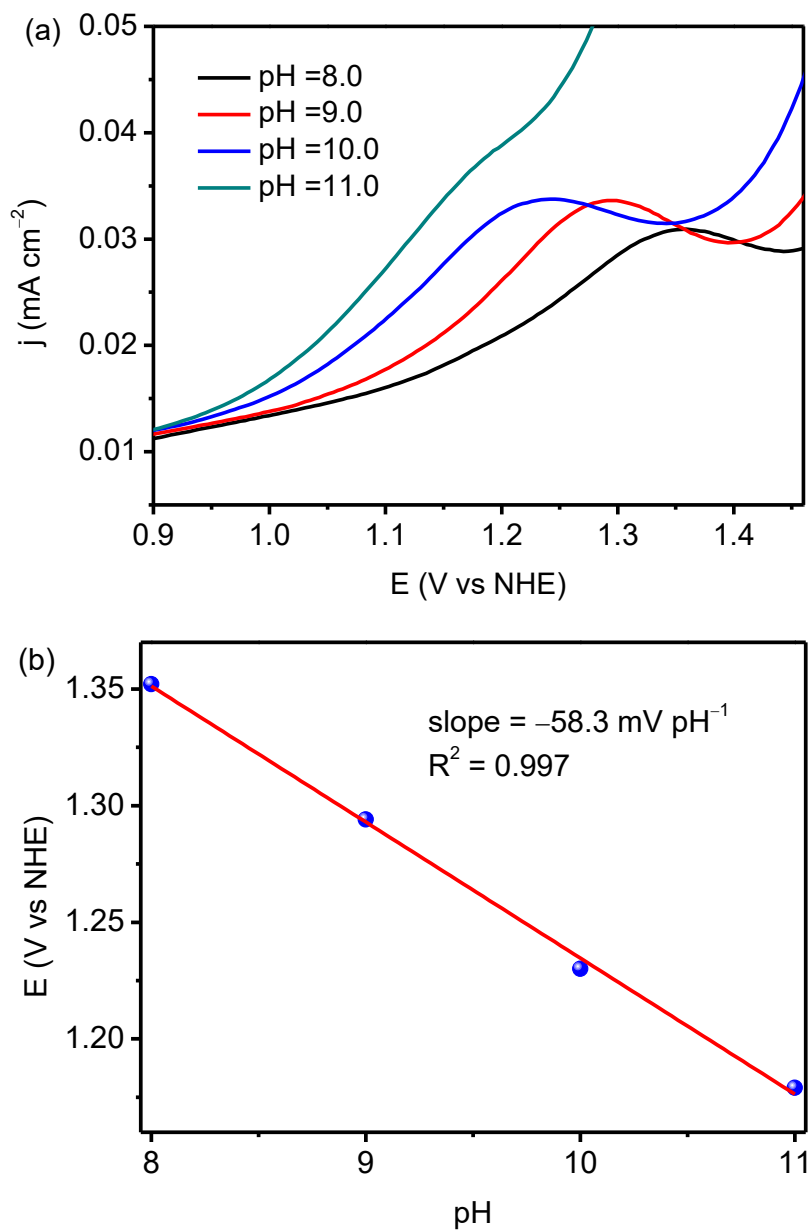
Figure S15. (a) DPV of $[Zn(N_2Py_3)]^{2+}$ (1.0 mM) in 0.1 M PBSs with pH varied from 8 to 11. (b) Pourbaix plots for $[Zn(N_2Py_3)]^{2+}$.
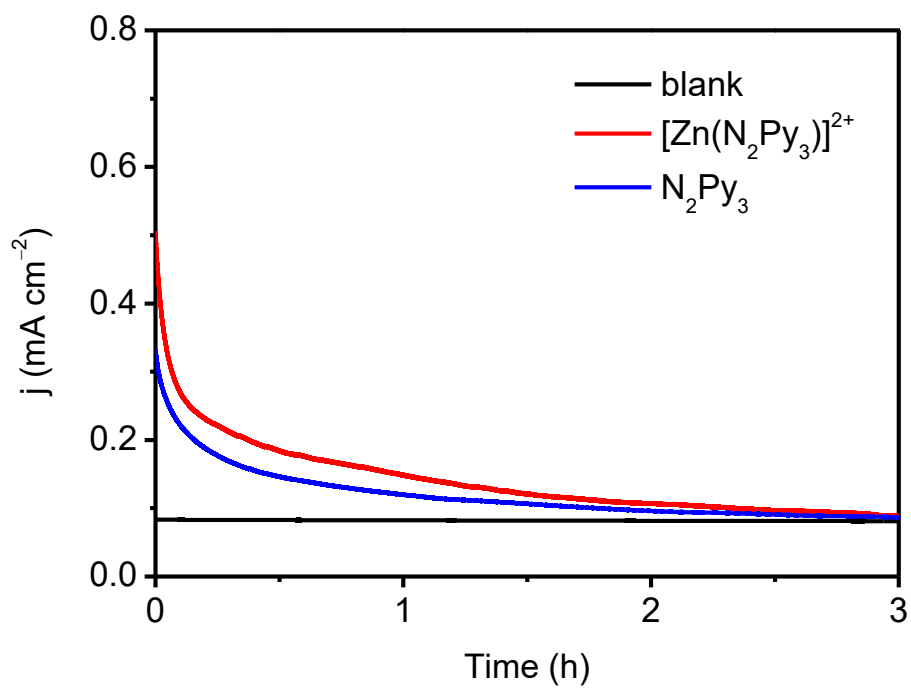
Figure S16. Catalytic currents of $[Zn(N_2Py_3)]^{2+}$ (1.0 mM), N_2Py_3 (1.0 mM), and blank

collected from CPE experiments at 1.6 V vs. NHE in 0.1 M PBSs at pH 11.0.
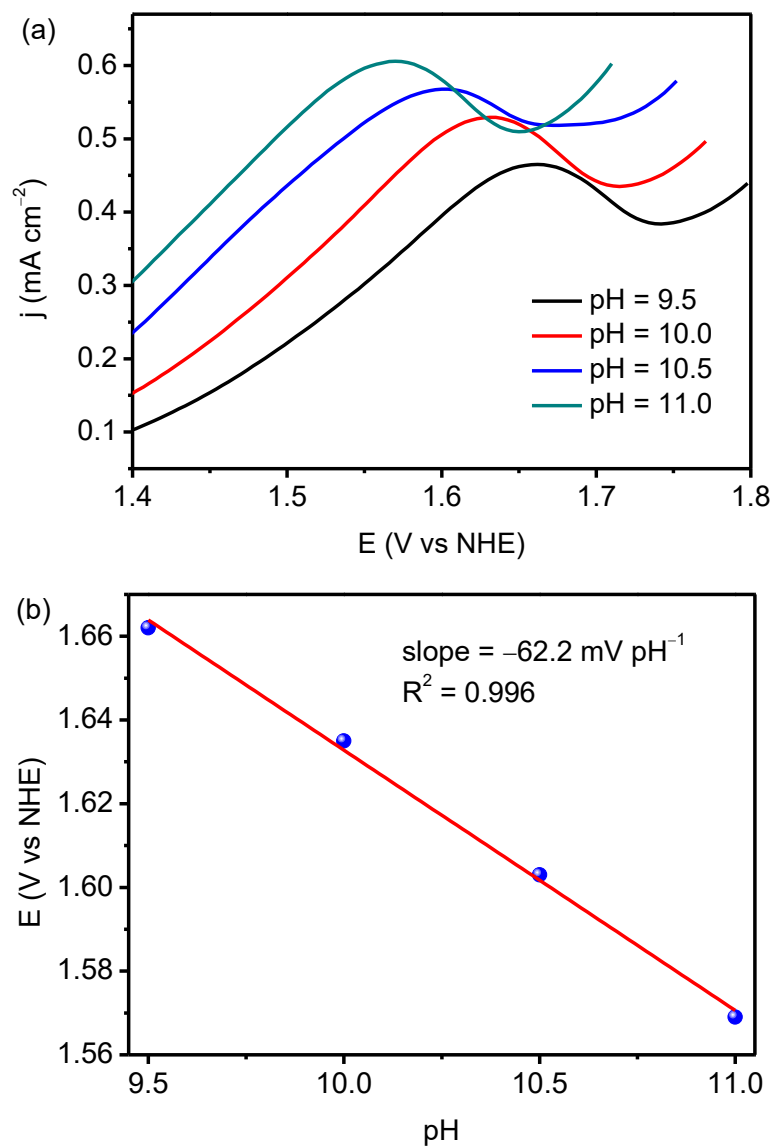
Figure S17. (a) DPV of the second oxidation peak for **1** (1.0 mM) in 0.1 M PBSs with

pH varied from 9.5 to 11. (b) Pourbaix plots of the second oxidation peak for **1**.
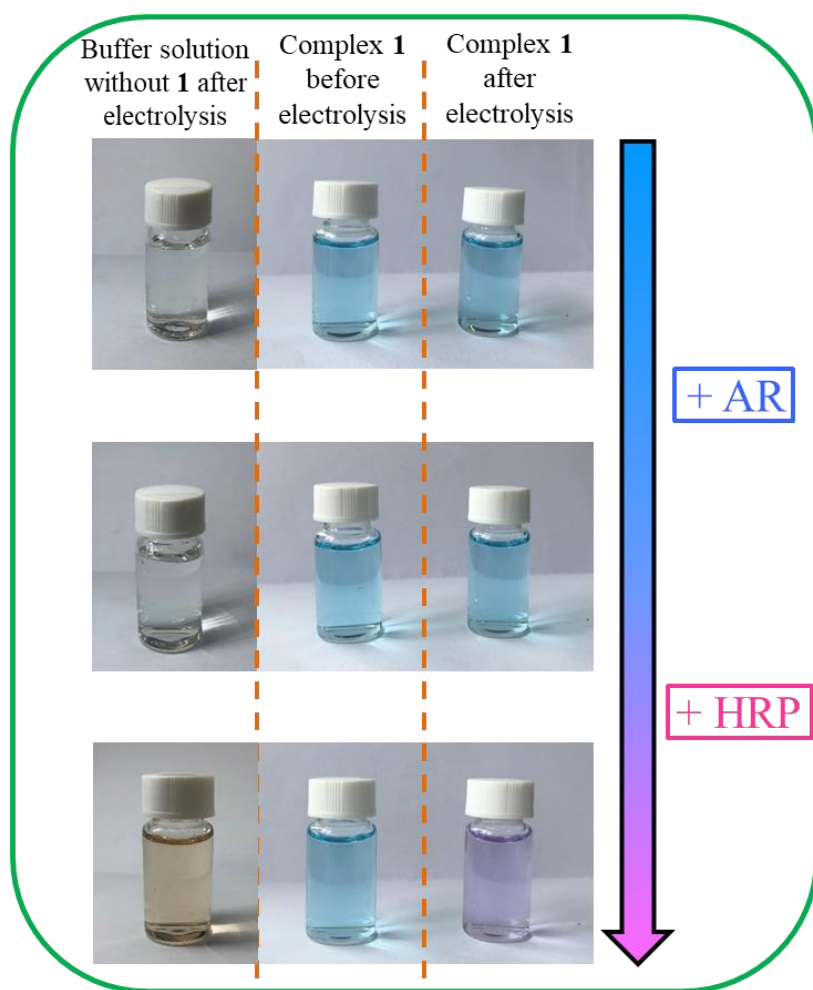
Figure S18. Experiments for testing the peroxide intermediates in the resulting electrolytes after 3 h electrolysis of **1** in 0.1 M PBSs at pH 11.0 by the addition of horseradish peroxidase (HRP, a special catalyst for hemolysis of the peroxide bond of H_2O_2 to form $^{\bullet}OH$ radicals) and Ampliflu red (AR, a reliable titrant for $^{\bullet}OH$).
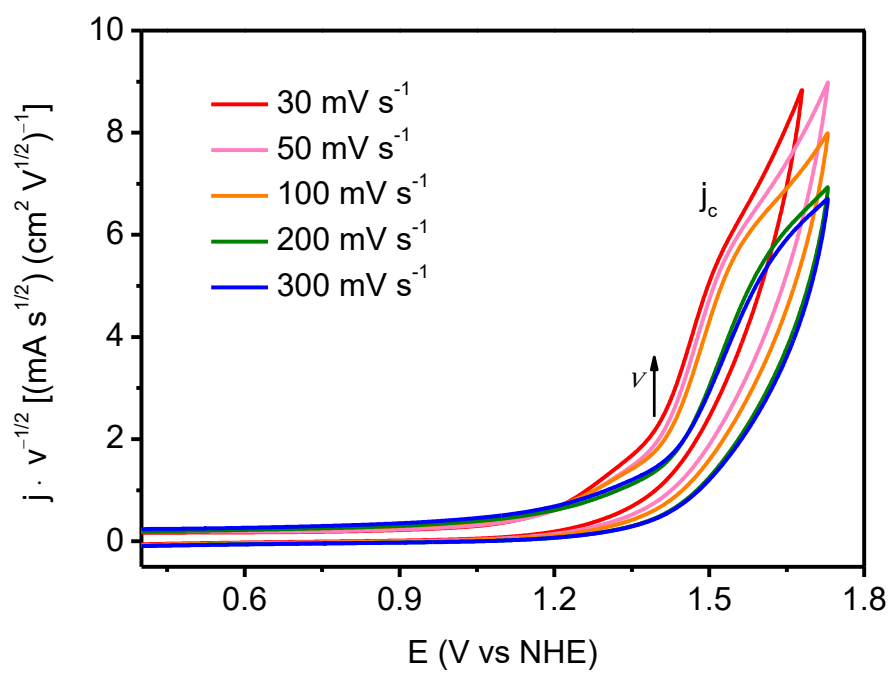
Figure S19. Catalytic current density responses of **1** (1.0 mM) in 0.1 M PBS at pH 11 normalized with $v^{1/2}$.
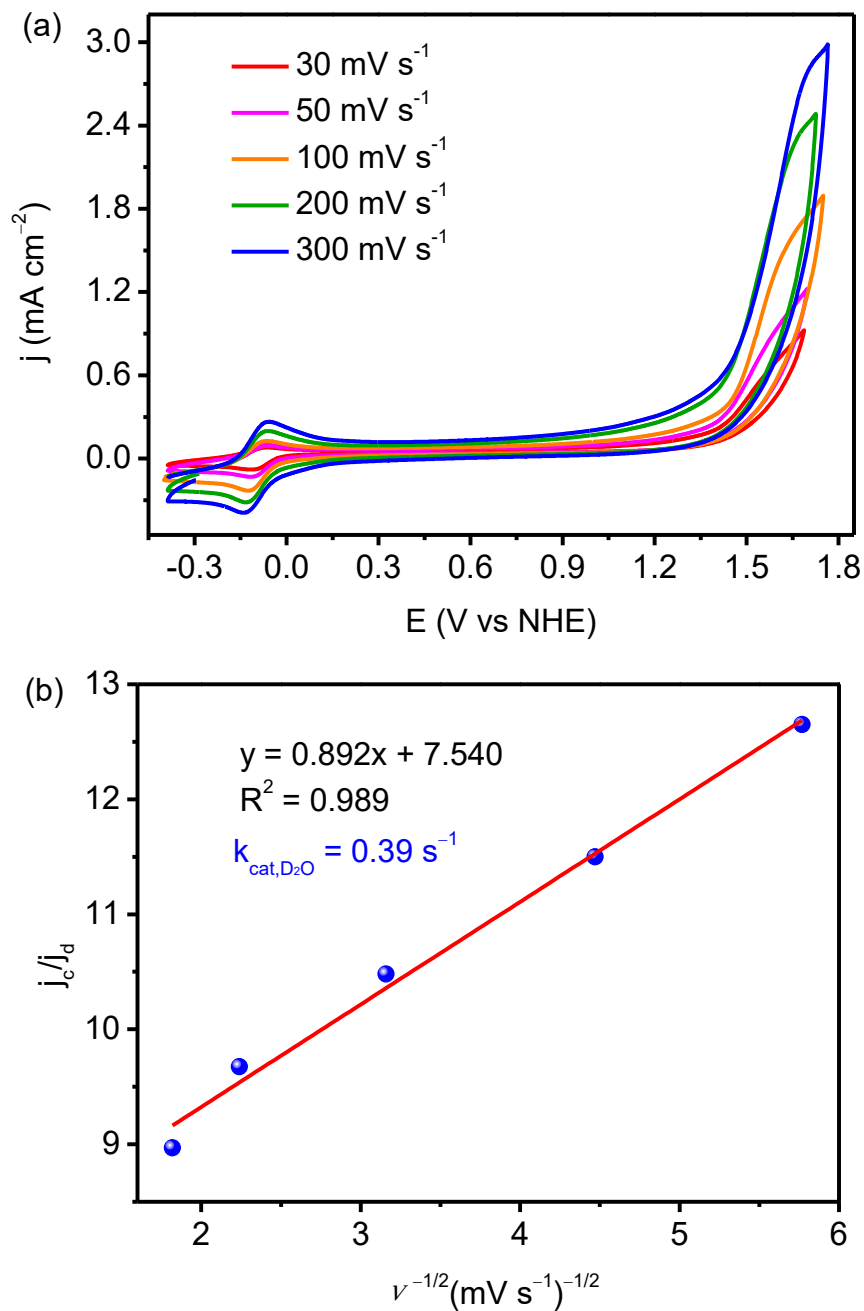
Figure S20. (a) Cyclic voltammogram of **1** (1.0 mM) in 0.1 M phosphate buffer D_2O solution at pD 11 at different scan rates (30–300 mV s^{-1}). (b) Plots of the ratio of j_c to j_d versus the reciprocal of the square root of scan rate. According to the equation of $KIE = k_{cat,H_2O}/k_{cat,D_2O}$, the value of KIE for **1** is 2.1.

Figure S21. (a) Cyclic voltammograms of **1** at a scan rate of 100 mV s^{-1} with the concentration of phosphate buffer solution varied from 0.025 to 0.1 M at pH 11. (b) Plots of $(j_c/j_d)^2$ as a function of $[HPO_4^{2-}]$ at constant concentration of **1**.

Table S1 Crystallographic data and processing parameters for **1**

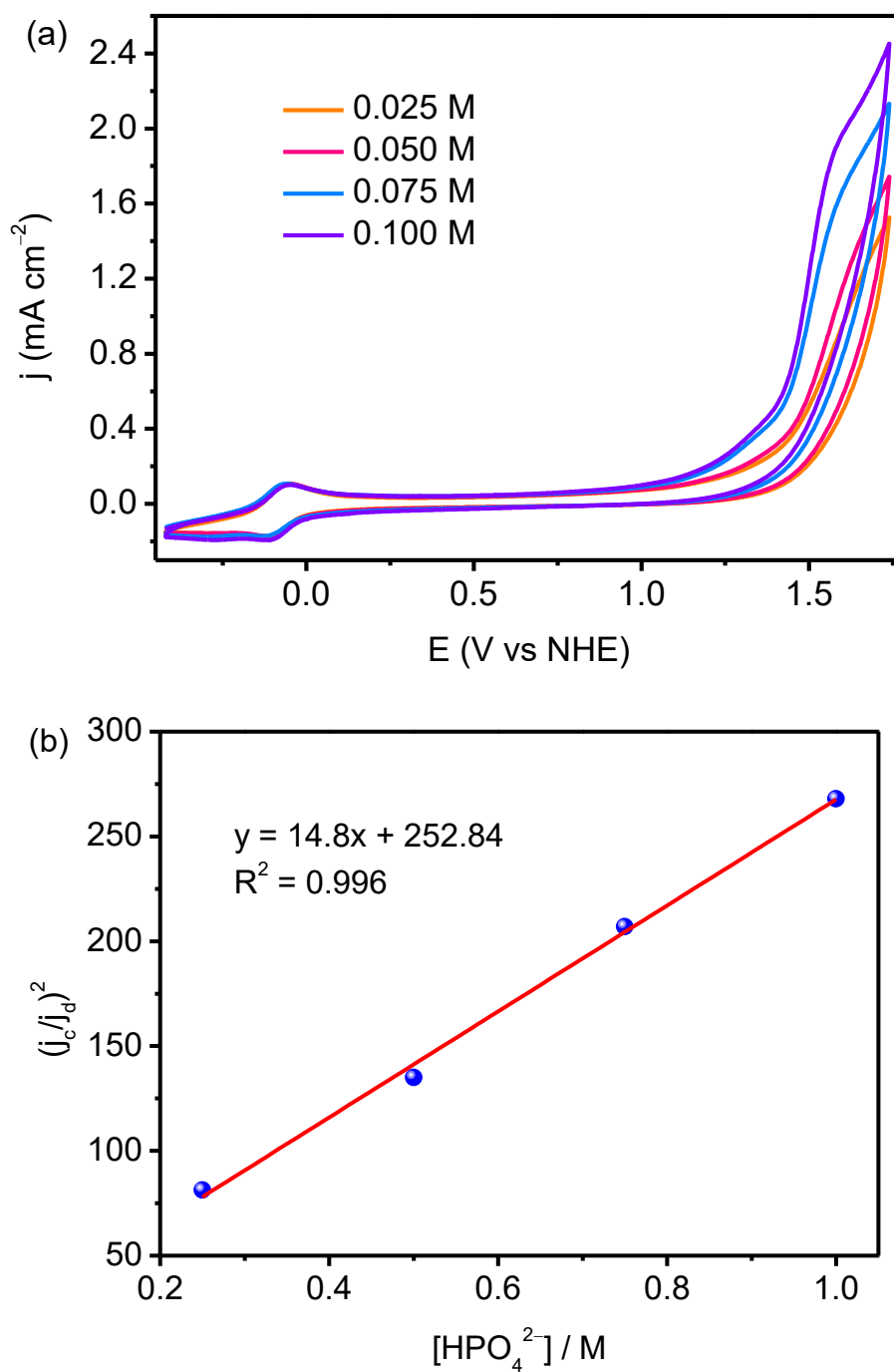| Complex	$[Cu(N_2Py_3)](BF_4)_2$
Formula	$C_{21}H_{25}N_5B_2F_8Cu$
Formula weight	584.62
Crystal system	Monoclinic
Space group	*C2/c*
Z	4
a / Å	14.002(4)
b / Å	11.085(3)
c / Å	15.701(4)
α / deg	90.00
β / deg	94.935(5)
γ / deg	90.00
V / Å^3	2428.0(11)
D_{calcd} / g m^{-3}	1.599
μ / mm^{-1}	0.982
Crystal size / mm	$0.21 \times 0.20 \times 0.19$
θ Range / deg	2.60 / 27.64
Reflns collected / Indep.	2518 / 2817
Parameters refined	170
$F(000)$	1188
GOF on F^2	1.146
Final R_1 ($I > 2(I)$)	0.0438
Final wR_2 ($I > 2(I)$)	0.1306
max. peak/hole / e Å^{-3}	0.623, -0.603

$$R_1 = \Sigma||F_o| - |F_c||/\Sigma|F_o|, \ wR_2 = [\Sigma(|F_o|^2 - |F_c|^2)^2/\Sigma(F_{o2})]^{1/2}$$

Table S2 Selected bond lengths (Å) and angles (deg) for **1**

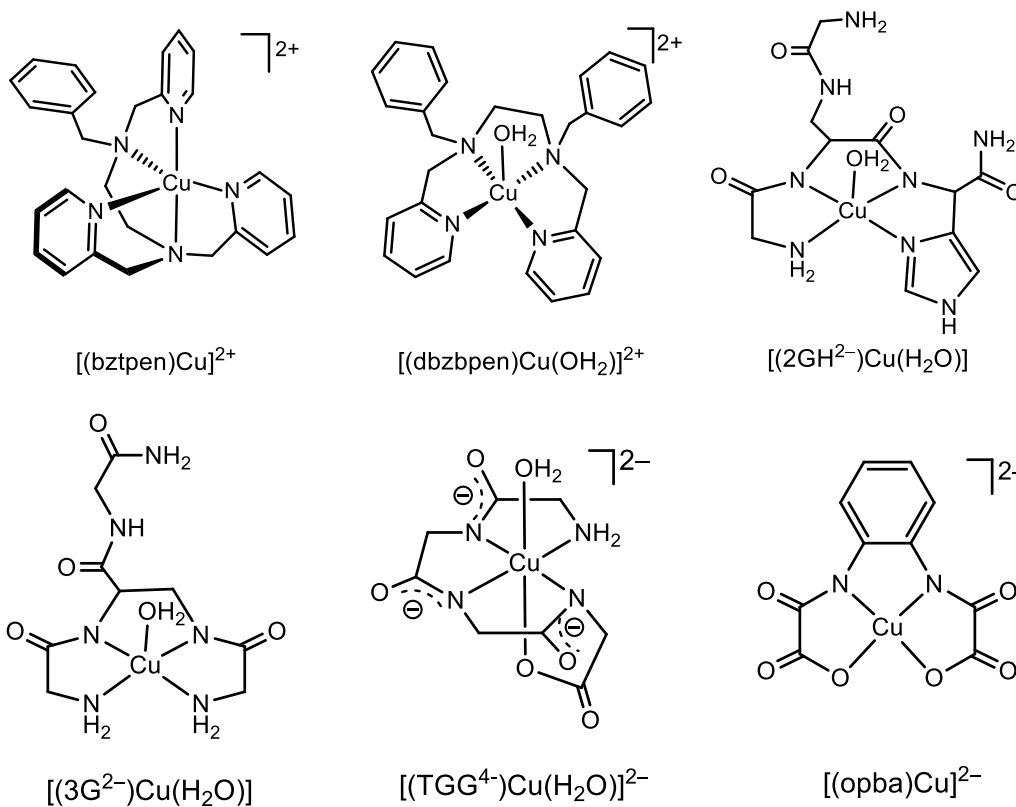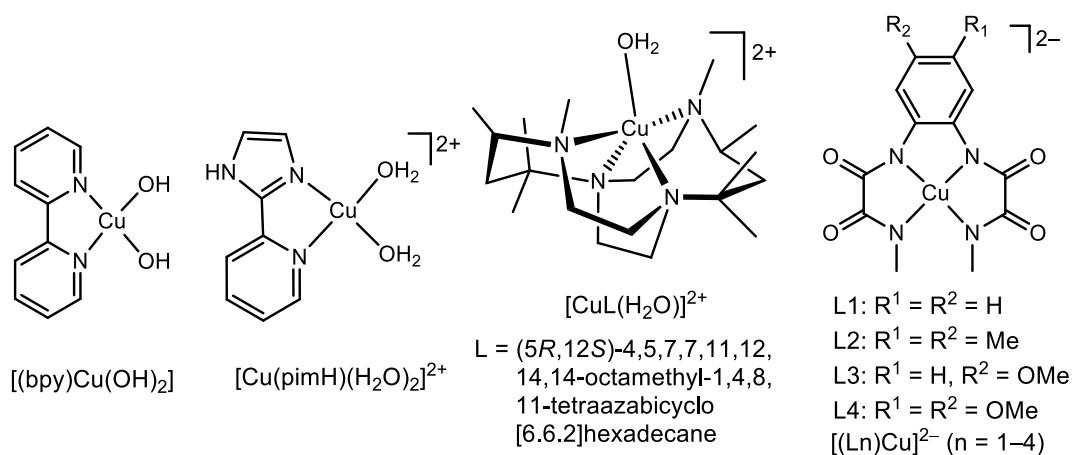| $[Cu(N_2Py_3)]^{2+}$	
Bond lengths (Å)	
Cu–N1	1.942(2)
Cu–N2	2.069(2)
Cu–N3	2.095(2)
Cu–N4	2.095(2)
Cu–N5	2.069(2)
Bond angles (deg)	
N1–Cu–N2	80.89 (5)
N1–Cu–N3	130.73(5)
N1–Cu–N4	130.73(5)
N1–Cu–N5	80.89 (5)
N2–Cu–N3	80.72(7)
N2–Cu–N4	111.57(7)
N2–Cu–N5	161.79(1)
N3–Cu–N4	98.84(2)
N3–Cu–N5	111.58(7)
N4–Cu–N5	80.73(7)

Table S3 Overpotentials and observed rate constants for mononuclear copper complexes reported as WOCs in alkaline aqueous solution (pH from 10 to 14)

Entry	Catalyst[a]	pH	η (half peak overpotential) (mV)[b]	k_{cat} (s^{-1})	Ref.
1	[(6,6′-2O⁻-bpy)Cu(H₂O)₂]	12–14	510–560	0.4 (pH 12.4)	S4
2	[Cu(pyalk)₂]	13.3	607	0.7	S5
3	[(6,6′-dhbp)₂Cu(CH₃OH)]²⁺	12.6	516	0.356	S6
4	[(bpy)Cu(OH)₂]	12.5	750	100	S7
5	[Cu(pimH)(H₂O)₂]²⁺	12	780	35	S8
6	[CuL(H₂O)]²⁺	12	680	–	S9
7	[(L1)Cu]²⁻	11.5	700	3.56	S10
8	[(L2)Cu]²⁻	11.5	400	3.58	S10
9	[(L3)Cu]²⁻	11.5	270	0.43	S10
10	[(L4)Cu]²⁻	11.5	170	0.16	S10
11	[(bztpen)Cu]²⁺	11.5	950	13.1	S11
12	[(dbzbpen)Cu(OH₂)]²⁺	11.5	850	18.7	S11
13	[(2GH²⁻)Cu(H₂O)]	11	803	53	S12
14	[(3G²⁻)Cu(H₂O)]	11	771	24	S12
15	[(TGG⁴⁻)Cu(H₂O)]²⁻	11	621	33	S13
16	[(opba)Cu]²⁻	10.8	1010	1.13	S14
17	[pdca–Cu^{II}–CO₃H]⁻	10	762	20.1	S15
18	[(N₂Py₃)Cu]²⁺ (**1**)	11	831	0.83	This work

[a] The structures of the catalysts listed in Table S3 are given below.
[b] The half peak overpotentials of several WOCs are estimated in their CV curves.

[(6,6'-2O⁻-bpy)Cu(OH)₂]²⁻   Cu(pyalk)₂   [(6,6'-dhbp)₂Cu(CH₃OH)]²⁺   [pdca-Cu^{II}-CO₃H]⁻

L = CH₃OH

[(bpy)Cu(OH)₂]

[Cu(pimH)(H₂O)₂]²⁺

[CuL(H₂O)]²⁺

L = (5*R*,12*S*)-4,5,7,7,11,12,
14,14-octamethyl-1,4,8,
11-tetraazabicyclo
[6.6.2]hexadecane

L1: R¹ = R² = H
L2: R¹ = R² = Me
L3: R¹ = H, R² = OMe
L4: R¹ = R² = OMe
[(Ln)Cu]²⁻ (n = 1–4)

[(bztpen)Cu]²⁺

[(dbzbpen)Cu(OH₂)]²⁺

[(2GH²⁻)Cu(H₂O)]

[(3G²⁻)Cu(H₂O)]

[(TGG⁴⁻)Cu(H₂O)]²⁻

[(opba)Cu]²⁻
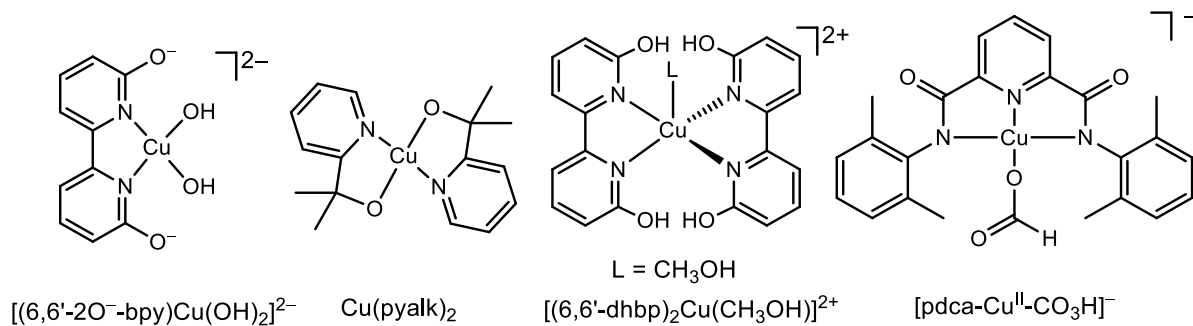
References

S1 G. M. Sheldrick, SHELXTL97 Program for the Refinement of Crystal Structure, University of Göttingen, Germany, 1997.

S2 Software packages SMART and SAINT, Siemens Energy & Automation Inc., Madison, Wisconsin, 1996.

S3 G. M. Sheldrick, SADABS Absorption Correction Program, University of Göttingen, Germany, 1996.

S4 T. Zhang, C. Wang, S. Liu, J.-L. Wang and W. Lin, *J. Am. Chem. Soc.* 2014, **136**, 273−281.

S5 K. J. Fisher, K. L. Materna, B. Q. Mercado, R. H. Crabtree and G. W. Brudvig, *ACS Catal.* 2017, **7**, 3384−3387.

S6 D. L. Gerlach, S. Bhagan, A. A. Cruce, D. B. Burks, I. Nieto, H. T. Truong, S. P. Kelley, C. J. Herbst-Gervasoni, K. L. Jernigan, M. K. Bowman, S. Pan, M. Zeller and E. T. Papish, *Inorg. Chem.* 2014, **53**, 12689−12698.

S7 S. M. Barnett, K. I. Goldberg and J. M. Mayer, *Nat. Chem.* 2012, **4**, 498−502.

S8 L. A. Stott, K. E. Prosser, E. K. Berdichevsky, C. J. Walsby and J. J. Warren, *Chem. Commun.* 2017, **53**, 651−654.

S9 J. Wang, H. Huang and T. Lu, *Chin. J. Chem.* 2017, **35**, 586−590.

S10 P. Garrido-Barros, I. Funes-Ardoiz, S. Drouet, J. Benet-Buchholz, F. Maseras and A. Llobet, *J. Am. Chem. Soc.* 2015, **137**, 6758−6761.

S11 J. Shen, M. Wang, P. Zhang, J. Jiang and L. Sun, *Chem. Commun.* 2017, **53**, 4374−4377.

S12 J. S. Pap, L. Szyrwiel, D. Sranko, Z. Kerner, B. Setner, Z. Szewczuk and W. Malinka, *Chem. Commun.* 2015, **51**, 6322−6324.

S13 M.-T. Zhang, Z. Chen, P. Kang and T. J. Meyer, *J. Am. Chem. Soc.* 2013, **135**, 2048−2051.

S14 L.-Z. Fu, T. Fang, L.-L. Zhou and S.-Z. Zhan, *RSC Adv.* 2014, **4**, 53674−53680.

S15 F. F. Chen, N. Wang, H. T. Lei, D. Y. Guo, H. F. Liu, Z. Y. Zhang, W. Zhang, W. Z. Lai and R. Cao, *Inorg. Chem.*, 2017, **56**, 13368–13375.